Journal of Alloys and Compounds 509 (2011) 3717–3722

Contents lists available at ScienceDirect

Journal of Alloys and Compounds

journal homepage: www.elsevier.com/locate/jallcom

Effect of high temperature sintering on the structural and the magnetic properties of $La_{1.4}Ca_{1.6}Mn_2O_7$

E. Taşarkuyu[a,*], A. Coşkun[a], A.E. Irmak[a], S. Aktürk[a], G. Ünlü[a], Y. Samancıoğlu[a], A. Yücel[a], C. Sarıkürkçü[b], S. Aksoy[c], M. Acet[c]

[a] Department of Physics, Faculty of Sciences and Letters, Muğla University, 48000 Kötekli, Muğla, Turkey
[b] Department of Chemistry, Faculty of Sciences and Letters, Muğla University, 48000 Kötekli, Muğla, Turkey
[c] Experimental Physics, Duisburg-Essen University, 47048 Duisburg, Germany

ARTICLE INFO

Article history:
Received 13 October 2010
Received in revised form
30 November 2010
Accepted 2 December 2010
Available online 10 December 2010

Keywords:
Perovskite manganites
Sintering temperature
Magnetocaloric effect
Curie temperature

ABSTRACT

We investigate the effect of sintering temperature on the structural and magnetic properties of $La_{1.4}Ca_{1.6}Mn_2O_7$ double perovskite manganite compound prepared by the sol–gel route. Three sintering temperatures (1273, 1473 and 1673 K) are utilized for the heat treatment. Regardless of the sintering temperature, the tetragonal crystal structure with the *I*4/*mmm* space group is stable. However, a reduction in *a* and an increase in *c* lattice parameters along with a significant increase in crystallite-size occur on increasing the sintering temperature. This is also accompanied by the growth of grains. Grain-growth and changing crystallite-sizes account for the changes in magnetization, Curie temperature and magnetic entropy-change values. As the sintering temperature increases from 1273 to 1673 K the Curie temperature increases from 225 to 268 K and the magnetic entropy-change increases from 0.58 to 3.1 J kg^{-1} K^{-1} respectively.

1. Introduction

Magnetic cooling technology, in spite of some of its practical difficulties, can be an alternative to the commonly used vapor compression technology. In recent studies, it has been found that manganite compounds in the chemical form of $La_{1-x}A_xMnO_3$ (*A* is a monovalent ion such as Na, Li, Ag and K or a divalent ion such as Ca, Sr, Ba and Pb) exhibit large magnetocaloric effects (MCE) around room temperature [1–3]. These compounds exhibit a large magnetic entropy change (ΔS_M) around the paramagnetic (PM)–ferromagnetic (FM) phase transition at the Curie temperatures T_C lying close to room temperature and large relative cooling power (RCP) so as to justify their potential use in technological applications. Apart from the above-mentioned manganites, another family of compounds in the form $La_3B_2O_7$, the so called the double perovskite manganites (where *B* is Ca, Sr, Ba etc.), have also been studied extensively [4–7]. This class of materials exhibits differences from the classical ABO_3 type perovskite materials by their layered structure and anisotropic exchange interactions. The two-dimensional magnetic ordering and the colossal magnetoresistance (CMR) effect at low temperatures are other distinctive and intriguing properties of these materials. High magnetic entropy change at low magnetic field changes and tunable magnetic phase transition properties make these materials good candidates as working elements in magnetic refrigeration applications. Additionally, ease of preparation, low cost, grain growth to a desired size via heat treatment, and high chemical stability are some other advantageous properties of these materials for use in magnetic refrigeration systems. There are intensive studies on these materials which are reported in the literature, and some of them are listed in Table 1 [6–11]. It is interesting to note that samples reported to have similar compositions have different T_C and ΔS_M values which appears to be due to varying preparation conditions. This is particularly evident in the case of $La_{1.4}Ca_{1.6}Mn_2O_7$ in which the Curie temperature varies in a broad temperature range of 200–270 K. This indicates that it could be possible to optimize or tune the magnetic properties by adjusting the preparation conditions.

Therefore, in the present work, we have investigated the effect of the sintering temperature T_s (1273, 1473, and 1673 K) of $La_{1.4}Ca_{1.6}Mn_2O_7$ on its structural and the magnetic properties and on the magnetocaloric effects.

2. Experimental procedure

In order to obtain homogeneous samples, the $La_{1.4}Ca_{1.6}Mn_2O_7$ compound has been prepared by the sol–gel method. Appropriate amounts of La_2O_3, $CaCO_3$, and $Mn(NO_3)_2{\cdot}4H_2O$ were dissolved in dilute HNO_3 at 423 K. Then citric acid and ethylene glycol were added to the mixture. A viscous residue was formed by slowly boiling this solution at 473 K. The residue was dried slowly at 573 K until a dry-gel was

* Corresponding author. Tel.: +90 2522111597.
E-mail address: etasarkuyu@gmail.com (E. Taşarkuyu).

0925-8388/$ – see front matter © 2010 Elsevier B.V. All rights reserved.
doi:10.1016/j.jallcom.2010.12.011

Table 1
Comparison of magnetocaloric properties some double perovskite $La_{3-x}A_xMn_2O_7$ compounds.

Compounds	T_C (K)	ΔS_M (J kg^{-1} K^{-1})	H (T)	Preparation technique	Sintering temp. (K)	Ref.
$La_{1.4}Sr_{1.6}Mn_2O_7$	161	2.0	2	Sol–gel	1273	[6]
$La_{1.4}(Sr_{0.8}Ba_{0.2})_{1.6}Mn_2O_7$	125	2.25	1	Sol–gel	1273	[6]
$La_{1.4}(Sr_{0.4}Ba_{0.6})_{1.6}Mn_2O_7$	91	2.84	2	Sol–gel	1273	[6]
$La_{1.4}Ca_{1.6}Mn_2O_7$	215	2.28	1	Solid state	1673	[7]
$La_{1.4}Sr_{0.6}Ca_{1.0}Mn_2O_7$	320	0.84	2	Solid state	1673	[7]
$La_{1.4}Sr_{0.2}Ca_{1.4}Mn_2O_7$	268	1.20	2	Solid state	1673	[7]
$La_{1.4}Ca_{1.6}Mn_2O_7$	270	11.3	2	Solid state	1430	[8]
$La_{1.4}Ca_{1.6}Mn_2O_7$	200	–	–	Sol–gel	1273	[9]
$La_{1.34}Sr_{1.66}Mn_2O_7$	118	1.55	1	Sol–gel	1450	[10]
$La_{2.25}K_{0.75}Mn_2O_{7+\delta}$	235	1.3	1	Sol–gel	1473	[11]
$La_{2.05}K_{0.95}Mn_2O_{7+\delta}$	254	1.1	1	Sol–gel	1473	[11]
$La_{2.15}K_{0.85}Mn_2O_{7+\delta}$	247	1.4	1	Sol–gel	1473	[11]

formed. Finally, it was burned in air at 873 K in order to remove organic materials produced during the chemical reactions. The material obtained from this process was ground to fine powder using an agate mortar. Three pellets of 13 mm diameter and 2 mm thickness were produced by pressing under a pressure of 3 tons. Each pellet was separately sintered at 1273, 1473, and 1673 K for 24 h in air and cooled down to room temperature in the furnace. The morphological, crystallographic and compositional properties of the samples were investigated by scanning electron microscopy with energy dispersive spectroscopy (SEM-EDS) and X-ray diffraction (XRD) techniques.

Field and temperature dependencies of the magnetization $M(H)$ and $M(T)$ were measured using a Quantum Design MPMS superconducting quantum interference device magnetometer. $M(T)$ was measured under 50 Oe in zero-field-cooled (ZFC) and field-cooled (FC) sequences. In the ZFC sequence, the sample is first cooled down to 5 K under zero-field. Then, a measuring field of 50 Oe is applied, and the magnetization is measured up to 300 K. Subsequently, without removing the field, the magnetization is measured in the FC sequence down to 5 K. In order to determine the magnetocaloric properties, $M(H)$ measurements were made on increasing and decreasing fields between 0 and 5 T at constant temperatures around T_C in steps of about 5 K.

3. Results and discussion

3.1. XRD results

The crystal structures of the samples sintered at 1273, 1473 and 1673 K are investigated by XRD. The XRD patterns of the sintered samples are given in Fig. 1. These patterns reveal $Sr_3Ti_2O_7$-type tetragonal ($I4/mmm$) perovskite structure. Additionally, the XRD spectra of the samples sintered at 1273 and 1673 K possess low intensity reflections at $2\theta = 32^\circ$ and 37.2° indicating a CaO impurity phase [12]. Also, the XRD pattern of the sample sintered at 1473 K features a small reflection at $2\theta = 34^\circ$ related to a Mn_2O_3 impurity phase. All samples show a common reflection at $2\theta = 38.6^\circ$ that is related to a Mn_5O_8 phase.

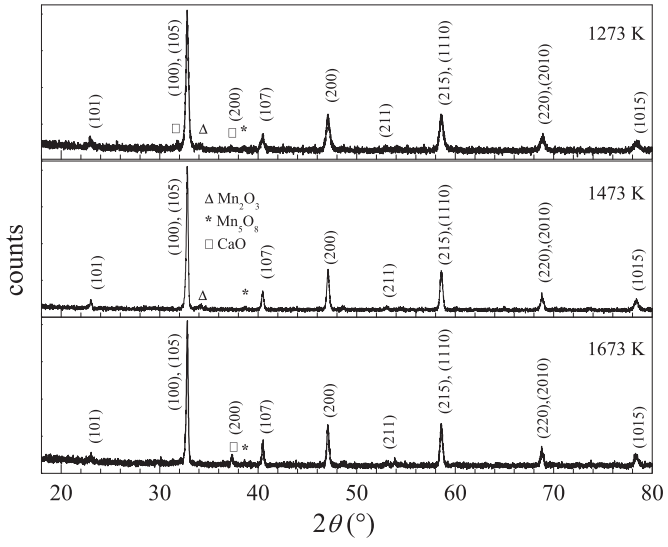

Fig. 1. XRD spectra of the samples sintered at 1273, 1473 and 1673 K for 24 h. The reflections are indexed according to the perovskite phase. Other minor reflections denoted by the symbols are related to impurity phases (see text).

From the XRD spectra of the samples, we calculate the lattice parameters, c/a ratios, unit-cell volumes, and crystallite-sizes. These are collected in Table 2. The variation of the c/a ratio and the unit cell volume and, similarly, the variation of a and c with T_s are given in Fig. 2(a) and (b) respectively. It is seen that a slowly decreases while c slowly increases for a change in T_s from 1273 to 1473 K. However, when T_s is raised from 1473 to 1673 K, the changes in a and c become more pronounced. An abrupt increase in c and a sharp decrease in a can be attributed to a Jahn–Teller distortion of the MnO_6 octahedra, indicating that the e_q electron is in the $d_{3z^2-r^2}$ orbital. A similar behavior is seen for the c/a ratio and the unit cell volume. The spectra in the vicinity of the (1 0 0) major reflections in Fig. 1 are plotted separately in Fig. 3 to emphasize the change in width with changing T_s. Broadening is observed for $T_s = 1273$ K with respect to the spectra pertaining to the other two sintering temperatures. The average crystallite-sizes calculated using the Debye–Scherrer formula are given in Table 2 and also plotted in Fig. 7 as a functions of T_s.

3.2. SEM and EDS analysis

The morphologies of the samples sintered at different temperatures were investigated by SEM, and the images are given in Fig. 4(a)–(c). The most notable feature of these images is the increase in grain-size with increasing sintering temperature. The average grain-sizes of samples sintered at 1273 and 1473 K are about 0.3 and 1 μm respectively. However, the sample sintered at 1673 K has a mixture of large and small grains with the larger ones being around 3 μm and the smaller ones around 1 μm. Additionally, the sample sintered at the lowest temperature has porosities between the grains. As a result of sintering at elevated temperatures, this porous structure disappears gradually, and a morphology with tightly connected grains and almost no porosity results.

3.3. Magnetic properties

Fig. 5(a)–(c) shows $M(T)$ under ZFC and FC conditions for an applied field of 50 Oe. The splitting is largest for the lowest T_s and

Table 2
Room temperature lattice parameters, c/a ratio, unit cell volume V, and crystallite-size of the samples.

T_s (°C)	a (Å)	c (Å)	c/a	V (Å^3)	Cryst. size (nm)
1273	3.8658	19.2769	4.9870	288.12	28.2
1473	3.8637	19.2790	4.9893	287.77	37.9
1673	3.8524	19.3436	5.0212	287.07	39.3

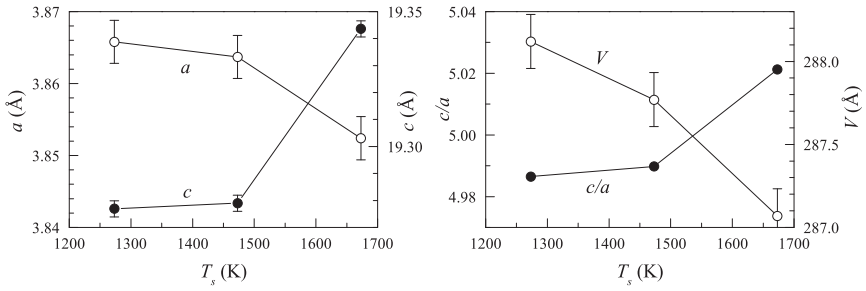

Fig. 2. Variation of (a) lattice parameters and (b) the c/a ratio and unit cell volume as a function of T_s.

increases as T_s increases. When measured under the FC condition in low fields such as 50 Oe, $M(T)$ at a PM-FM transition would be expected to increase sharply with decreasing temperature up to the demagnetizing limit and remain constant down to low temperatures. For the present system the transition is smeared over a broad temperature range for T_s = 1273 K and becomes sharper as T_s increases. T_C can be fairly well determined for T_s = 1473 and 1673 K to be 265 and 268 K, respectively. However, for T_s = 1273 K, we can only attribute a temperature range of 225–240 K for T_C.

In small external magnetic fields, the origin of the ZFC-FC splitting occurring close to or at T_C in a FM material can be related to the intrinsic magnetic anisotropy and to domain wall pinning in the magnetically ordered state so that applying a field, or not applying field, while cooling through T_C leads to different spin configurations that give rise to different net magnetizations. This effect can be particularly enhanced to lead to stronger domain wall pinning if non-FM inhomogeneities reside within the magnetic domain walls or within crystallite boundaries.

As T_s increases, so does the crystallite-size as seen in Fig. 4. For the case of maximum crystallite size (T_s = 1673 K), the splitting in $M(T)$ is smallest (Fig. 5), and the ZFC branch does not tend to a zero-value at low temperatures. This indicates that the dominant

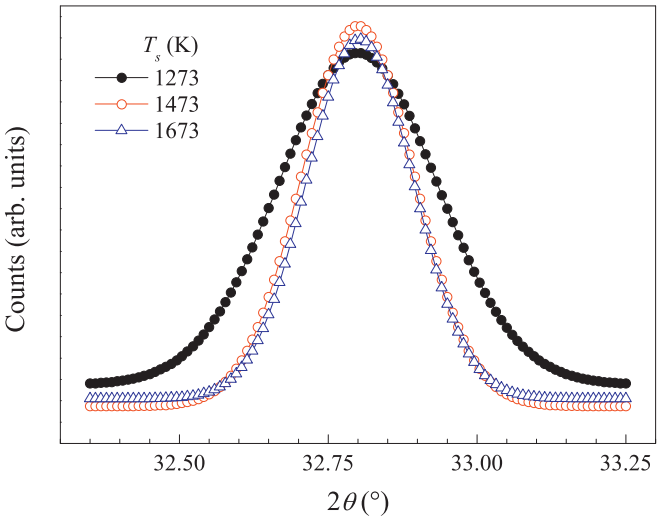

Fig. 3. Broadening of the (1 0 0) reflection at 2θ = 32.8° as a function of sintering temperature, T_s.

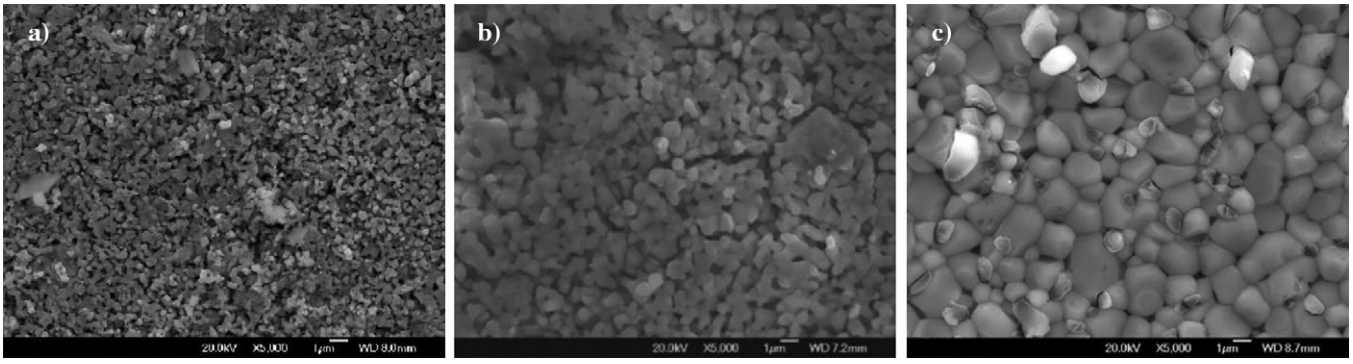

Fig. 4. SEM images of the samples sintered at (a) 1273 (b) 1473 and (c) 1673 K.

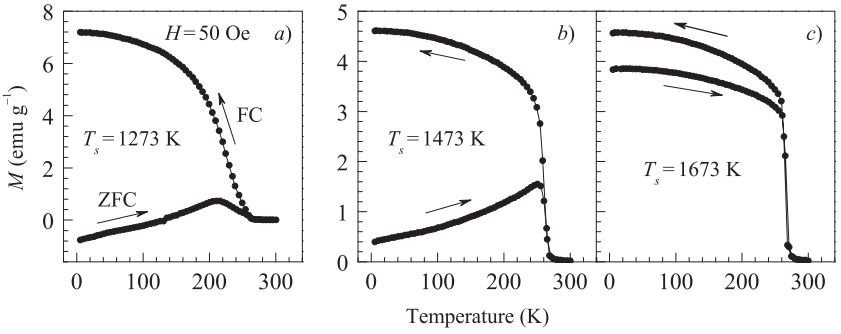

Fig. 5. $M(T)$ for $La_{1.4}Ca_{1.6}Mn_2O_7$ sintered at (a) 1273, (b) 1473, and (c) 1673 K.

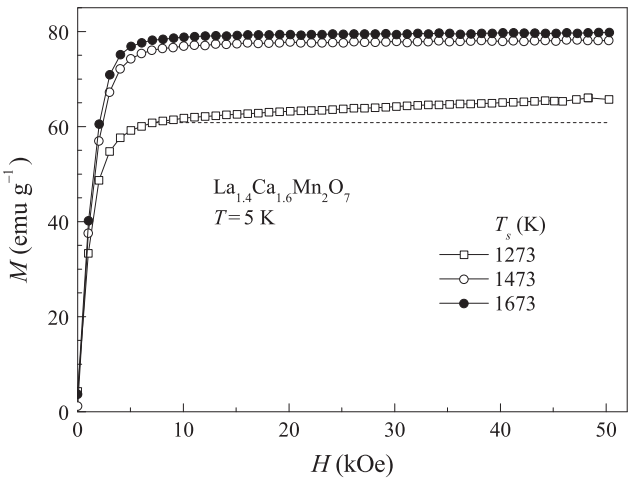

Fig. 6. Magnetization isotherms at 5 K. $M(H)$ saturates for T_s = 1473 and 1673 K, whereas there is considerable high-field susceptibility for T_s = 1273 K.

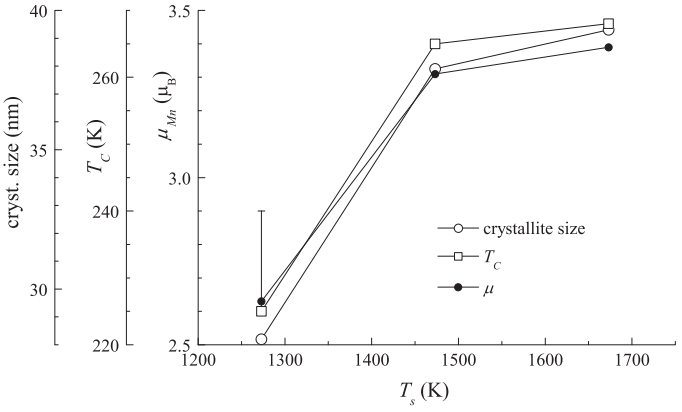

Fig. 7. Variation of the crystallite size, Curie temperature and the magnetic moment per Mn-atom with sintering temperature.

contribution to the splitting is from the FM anisotropy. In the case of the other two sintering temperatures where the crystallite sizes are smaller, the ZFC $M(T)$ tend to zero meaning that in addition to the FM anisotropy, non-FM entities, such as antiferromagnetic or non-collinear coupling, is also present giving rise to stronger domain wall pinning and thereby to a random moment configuration with vanishing net magnetization as $T \rightarrow 0$. As the temperature increases, the thermal energy gradually overcomes the anisotropy energy, and the ZFC-magnetization increases with increasing temperature up to T_C, above which pinning effects disappear.

The data in Fig. 5 together with the images in Fig. 4 show that in $La_{1.4}Ca_{1.6}Mn_2O_7$, larger grain-sizes are favorable for stronger long-range FM coupling. The presence of loosely connected, smaller grains result in a network of grain boundaries extending over lengthier distances than in the case of large grains. Grains with smaller sizes can create heavier strain at the grain boundaries and give rise to more non-FM or weak antiferromagnetic regions which can disturb the long-range FM order that is reflected in the size of T_C.

The average magnetic moment per Mn atom μ_{Mn} as a function of T_s is determined from the magnetization isotherms $M(H)$ in Fig. 6. The curves for T_s = 1473 and 1673 K show saturation, whereas considerable high-field susceptibility is found in the curve for T_s = 1273 K which can be seen by the deviation from saturation represented by the dashed line. μ_{Mn} is estimated from the curves to be 2.63, 3.31, and 3.39 μ_B per Mn atom for T_s = 1273, 1473, and 1673 K, respectively. The value at 1673 K is in good agreement with the bulk value [13].

The sintering temperature dependence of the crystallite size, T_C, and μ_{Mn} are plotted in Fig. 7. It is seen that these parameters show a similar increase with increasing T_s from 1300 to 1400 K after which they remain essentially constant. The magnetic properties such as T_C and the saturation magnetization of manganites depend on the c/a ratio, the average radius of the A-site ion, and the chemical pressure in the microstructure [13,14]. Here, it is seen that T_C increases by more than 20 K when T_s increases from 1273 to 1673 K. One possible explanation can be given by considering the effect of T_s on the lattice parameters, which, in turn, changes the Mn–O bond-length and the Mn–O–Mn bond-angle making Zener's double exchange interaction either stronger or weaker. As the c/a ratio increases, the double exchange interaction confines more to the ab-plane rather than in a plane perpendicular to it [7]. In the present case, the c/a ratio increases with increasing T_s (Fig. 2). Hence, it is understandable that the μ_{Mn} and T_C also increase with increasing T_s, i.e., through changing lattice parameters and, particularly in this case, through the suppression of non-FM entities as T_s increases. Similar behavior has also been observed in the work of Wang et al. [15].

3.4. Magnetocaloric effect

The magnetization isotherms between 0 and 5 T around the Curie temperatures and separated by 3 K-increments for the the samples sintered at 1273 and 1473 °C and 5 K-increments for the sample sintered at 1673 K are given in Fig. 8. Comparing the magnetization curves of the first two samples at low applied fields with that of the last sample, it is seen that the rate of change in magne-

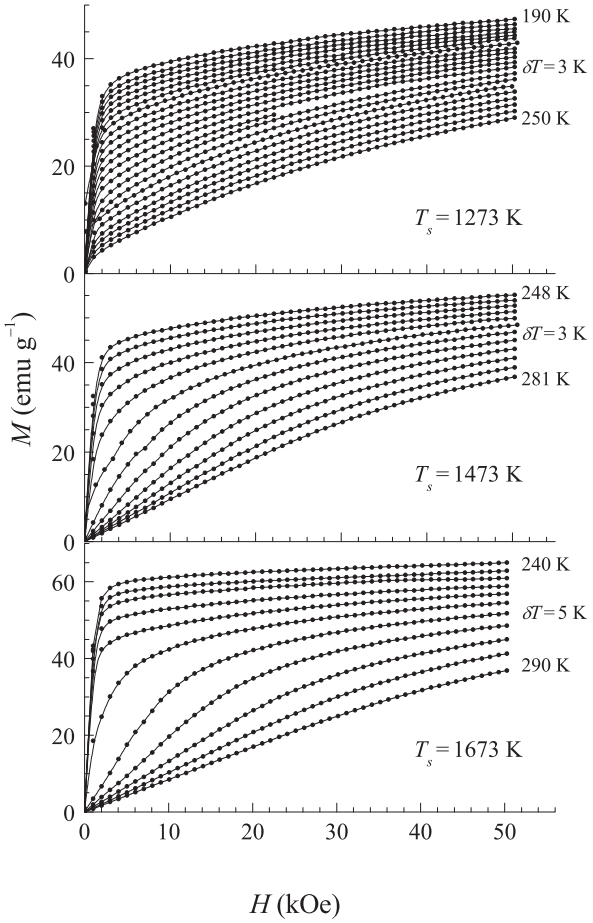

Fig. 8. $M(H)$ around T_C for $La_{1.4}Ca_{1.6}Mn_2O_7$ sintered at (a) 1273 K, (b) 1473 K, (c) 1673 K.

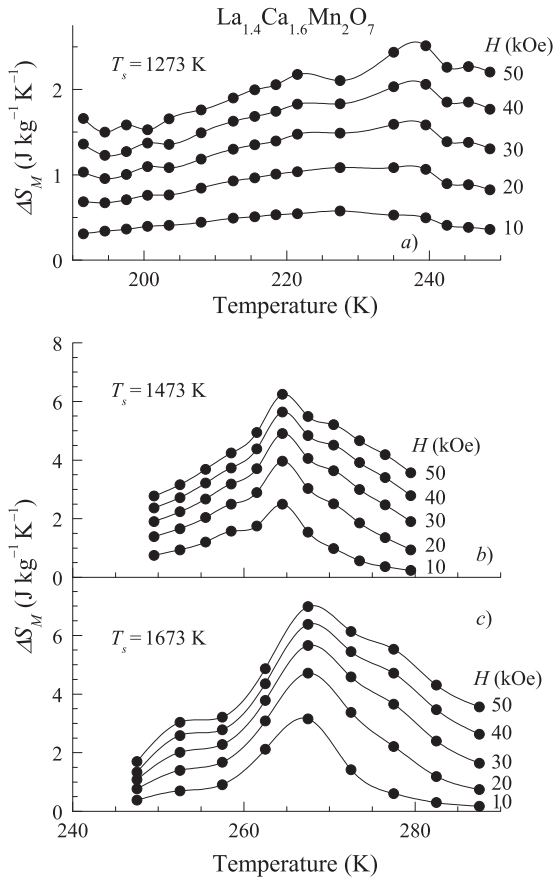

Fig. 9. The temperature dependence of ΔS for $La_{1.4}Ca_{1.6}Mn_2O_7$ sintered at (a) 1273, (b) 1473, and (c) 1673 K.

tization with respect to applied field just above T_C of the first two samples are more gradual than that of the latter. In contrast, for higher applied fields, the rate of change in magnetization is steeper for these two samples than the latter one. From these observations it can be deduced that the sample sintered at 1673 K should have a greater magnetic entropy change at lower field-change.

Isothermal magnetization measurements allow the calculation of the total magnetic entropy change, ΔS_M, of a sample through summing over discrete values of the magnetization isotherms such that

$$\Delta S_M = \sum_i \frac{M(T_{i+1}, H) - M(T_i, H)}{T_{i+1} - T_i} \Delta H. \quad (1)$$

In Fig. 9(a)–(c), the variations of entropy changes with respect to temperature corresponding to five different field changes are plotted. As seen, the magnetic entropy change becomes larger as T_s of the samples increases. The magnetic entropy changes under an applied magnetic field change of 1 T were calculated to be 0.58 J kg^{-1} K^{-1}, 2.5 J kg^{-1} K^{-1} and 3.1 J kg^{-1} K^{-1} for T_s of 1273, 1473 and 1673 K, respectively.

These magnetic entropy-change values belonging to the samples sintered at 1473 and 1673 K are greater than most values reported in the literature, except the one obtained by Zou et al. as listed in Table 1. Especially, the magnetic entropy change of the sample sintered at 1673 K as a function of temperature exhibits a broad variation with temperature around T_C. Such a variation covering a broad temperature range is beneficial for magnetic cooling applications. In cooling applications, the relative cooling power (RCP) is a good indicator of cooling efficiency of a magnetic refrigerant. The RCP corresponds to the amount of heat transferred between the cold and the hot sinks in the refrigeration cycle and is defined as $RCP(S) = \Delta S_{MAX} \times T_{FWHM}$, where ΔS_{MAX} is the maximum value of ΔS and T_{FWHM} is a full width at half maximum value of the temperature change. The RCP values for 1273, 1473, 1673 K sintered samples are calculated to be 55.0, 68.3, 81.6 J kg^{-1} K^{-1} respectively for a field change of 2 T. Therefore, the double perovskite $La_{1.4}Ca_{1.6}Mn_2O_7$ manganite compound, when sintered at elevated temperatures, can be considered to be a good candidate material for use as active element in magnetic refrigeration.

4. Conclusion

In this study, the $La_{1.4}Ca_{1.6}Mn_2O_7$ double perovskite manganite compound was prepared by the sol–gel method, and three samples were obtained from the prepared compound by sintering at 1273, 1473 and 1673 K. The effect of T_s on the structural and the magnetic properties were investigated. We observed through the XRD analysis that the lattice parameters and the crystallite-size were affected by sintering although the compositions remained nearly the same for all samples as determined by EDS. The c/a ratio of the tetragonal crystal structure has a tendency to increase with increasing T_s. The calculated crystallite-sizes increase with the increasing sintering temperature. The morphologies of the samples, investigated by SEM, also exhibit T_s-dependence. As with the crystallite-size, the grain-size tends to increase linearly with increasing T_s. Meanwhile, the porous structure seen on the sample sintered at 1273 K disappears gradually with increasing sintering temperature. An enhancement is observed in T_C with increasing T_s due to increasing grain and crystallite-sizes and decreasing porosities. The 1273 K-sintered sample has the smallest grain-size and is the most porous; therefore it has the greatest overall surface area that causes more magnetic scattering. It seems that for this reason, the 1273 K sintered sample has the lowest saturation magnetization, T_C and ΔS_M values among all the samples. Comparing to the 1273 K sintered sample, the 1473 K sample has less porosity and larger grains of about 1 μm in average. Despite containing some porosity, these closely touching grains cause this sample to have higher magnetization, T_C and ΔS_M values than those of the sample sintered at 1273 K. The sample sintered at 1673 K has the largest crystallite and grain-size and almost no porosity, and this sample displays superior magnetic properties as far as the magnetic cooling applications are considered. Consequently, it is plausible to conclude that T_s plays an important role in modifying physical properties of these materials in spite of the fact that the Mn^{3+}/Mn^{4+} ratio remains fixed by substituting La by a fixed amount of Ca in all samples.

Acknowledgments

The authors would like to acknowledge Erasmus Mobility Programme for supporting Gökhan Ünlü and Yusuf Samancoğlu at Experimentalphysik AG Farle Laboratory at Duisburg-Essen University.

References

[1] Z.B. Guo, Y.W. Du, J.S. Zhu, H. Huang, W.P. Ding, D. Feng, Phys. Rev. Lett. 78 (1997) 1142.
[2] W. Zhong, W. Chen, W.P. Ding, N. Zhang, Y.W. Du, Q.D. Yan, Solid State Commun. 106 (1998) 55.
[3] B.F. Yu, Q. Gao, B. Zhang, M.Z. Meng, Z. Chen, Int. J. Refrig. 26 (2003) 622.
[4] T. Murata, T. Terai, T. Fukuda, T. Kakeshita, J. Magn. Magn. Mater. 303 (2006) 138.
[5] A.K. Gupta, R. Kumar, V. Kumar, G.L. Bhalla, N. Khare, J. Phys. Chem. Solids 70 (2009) 117.
[6] K. Cherif, S. Zemni, J. Dhahri, M. Oumezzine, M. Said, H. Vincent, J. Alloys Compd. 432 (2007) 30.
[7] X. Zhao, W. Chen, Y. Zong, S.L. Diao, X.J. Yan, M.G. Zhu, J. Alloys Compd. 469 (2009) 61.

[8] H. Zhu, H. Song, Y. Zhang, Appl. Phys. Lett. 3416 (2002) 81.
[9] J.M. Dai, L.J. Zou, W.H. Song, Y. Ting, S.G. Wang, C.L. Yuan, S.L. Ye, S.Y. Wang, Y.P. Sun, Mater. Sci. Eng. B 76 (2000) 35.
[10] A. Wang, Y. Liu, Z. Zhang, Y. Long, G. Cao, Solid State Commun. 130 (2004) 293.
[11] W. Zhong, W. Chen, H.Y. Jiang, X.S. Liu, C.T. Au, Y.W. Du, Eur. Phys. J. B30 (2002) 331.
[12] M.M. Cruz, M.D. Carvalho, A. Casaca, G. Bonfait, F.M. Costa, M. Godinho, J. Magn. Magn. Mater. (2001) 226.
[13] H. Asano, J. Hayakawa, M. Matsui, Phys. Rev. B 56 (1997) 5395.
[14] M. Koubaa, W. Cheikhrouhou-Koubaa, A.W. Cheikhrouhou, J. Phys. Chem. Solids 70 (2009) 326.
[15] K. Wang, W. Song, T. Yu, B. Zhao, M. Pu, Y. Sun, Phys. Stat. Sol. A 171 (1999) 577.